

# Structural Studies and the Assembly of the Heptameric Post-translational Translocon Complex\*

Received for publication, June 29, 2010, and in revised form, September 7, 2010. Published, JBC Papers in Press, September 8, 2010, DOI 10.1074/jbc.M110.159517

Yoichiro Harada<sup>‡</sup>, Hua Li<sup>§</sup>, Joseph S. Wall<sup>§</sup>, Huilin Li<sup>‡§</sup>, and William J. Lennarz<sup>‡1</sup>

From the <sup>‡</sup>Department of Biochemistry and Cell Biology, Stony Brook University, Stony Brook, New York 11794 and the <sup>§</sup>Biology Department, Brookhaven National Laboratory, Upton, New York 11973-5000

In *Saccharomyces cerevisiae*, some of the nascent chains can be post-translationally translocated into the endoplasmic reticulum through the heptameric post-translational translocon complex (post-translocon). This membrane-protein complex is composed of the protein-conducting channel and the tetrameric Sec62/63 complex. The Sec62/63 complex plays crucial roles in targeting of the signal recognition particle-independent protein substrate to the protein-conducting channel and in assembly of the post-translocon. Although the molecular mechanism of the post-translational translocation process has been well established, the structure of the post-translocon and how the channel and the Sec62/63 complex form the heptameric complex are largely uncharacterized. Here, we report a 20-Å resolution cryo-electron microscopy structure of the post-translocon. The purified post-translocon was found to have a mass of 287 kDa, which is consistent with the unit stoichiometry of the seven subunits as determined by a cysteine labeling experiment. We demonstrated that Triton X-100 dissociated the heptameric complex into three subcomplexes identified as the trimeric translocon Sec61-Sbh1-Sss1, the Sec63-Sec71-Sec72 trimer, and the heterotetramer Sec62-Sec63-Sec71-Sec72, respectively. Additionally, a role of the sixth cytosolic loop of Sec61 in assembly of the post-translocon was demonstrated. Mutations of conserved, positively charged amino acid residues in the loop caused decreased formation of the post-translocon. These studies provide the first architectural description of the yeast post-translocon.

The process of protein translocation across the endoplasmic reticulum (ER)<sup>2</sup> membrane occurs co- or post-translationally (1). In the co-translational translocation pathway, the ribosomes with an emerging signal sequence are targeted to the ER membrane through a cytosolic peptide-targeting molecule called the signal recognition particle (SRP) and its receptor (the SRP-dependent pathway) (1, 2). In yeast, some signal sequences

are not recognized by SRP, and the nascent chains are fully synthesized in the cytosol where certain chaperones protect them from aggregation (3). These nascent chains may be post-translationally translocated into or across the ER membrane by a SRP-independent pathway.

The heterotrimeric Sec61 complex forms the protein-conducting channel for both co- and post-translational translocation of nascent chains in the ER membrane (1). In yeast, the channel is formed by three membrane proteins, Sec61, Sbh1, and Sss1 (see Fig. 1A, right panel). Sec61 consists of the core structure that has 10 transmembrane helices separated by nine loops (4, 5). Among the even-numbered loops (L2, L4, L6, and L8) facing the cytosol, the L8 loop contains a highly conserved, positively charged amino acid that provides a major binding site for the ribosomes (6, 7). The L6 loop plays a role in protein translocation by an unknown mechanism (6).

In the co-translational translocation mode, the association of the protein-conducting channel and the exit tunnel of the ribosomes allows direct passage of the nascent chains from the ribosomes through the ER membrane (7, 8). In the post-translational translocation mode, the protein-conducting channel partners with another membrane protein complex, called the tetrameric Sec62/Sec63 complex, consisting of Sec62, Sec63, Sec71, and Sec72 (see Fig. 1A, left panel) (9–12). Although the components that are required for the post-translational translocation process have been well characterized, the structure of the heptameric post-translocon and how it is assembled remain unknown.

To gain structural insights into molecular mechanisms underlying the post-translational translocation, we designed a new approach to efficiently purify the post-translocon from the yeast microsomes. Several lines of evidence based on cysteine labeling and EM analyses of the purified complex have shown that the post-translocon is composed of one copy of each subunit. Negative stain EM of the post-translocon containing Sec63 fused with maltose-binding protein suggested a location of the large cytosolic domain of Sec63 adjacent to the Sec61 channel. Mutagenesis of Sec61 indicated that the channel and the Sec62/63 complexes are assembled into the post-translocon via the sixth cytosolic loop of Sec61.

## EXPERIMENTAL PROCEDURES

**Materials**—Anti-HA antibody was purchased from Covance (Emeryville, CA). Anti-maltose-binding protein (MBP) antibody was purchased from Santa Cruz Biotechnology (Santa Cruz, CA). Triton X-100, EZ-view, anti-HA affinity gel, HA peptide, anti-FLAG, and biotinylated anti-FLAG antibodies

\* This work was supported, in whole or in part, by National Institutes of Health Grants GM33185 (to W. J. L.) and GM74985 (to H. L.). This work was also supported by Brookhaven National Laboratory Laboratory-directed Research and Development Grant 10-016 (to H. L.) and in part by the Department of Energy.

<sup>1</sup> To whom correspondence should be addressed: Dept. of Biochemistry and Cell Biology, State University of New York at Stony Brook, Stony Brook, NY 11794. Fax: 631-632-857; E-mail: wlennarz@notes.cc.sunysb.edu.

<sup>2</sup> The abbreviations used are: ER, endoplasmic reticulum; SRP, signal recognition particle; MBP, maltose-binding protein; BN, Blue Native; STEM, scanning transmission electron microscopy; SEC, heptameric post-translational translocon.

were purchased from Sigma. Digitonin was purchased from Calbiochem (Darmstadt, Germany). SDS-polyacrylamide gel was purchased from Bio-Rad. Q-Sepharose was purchased from GE Healthcare.

**Yeast Strains**—To generate the C-terminal triple HA-tagged Sec62 construct (designated as Sec62-HA), a PCR was carried out using pFA6a-3xHA-TRP1 (13) as a template, which was a kind gift from Dr. Rolf Sternglanz (Department of Biochemistry and Cell Biology, Stony Brook University). The primers were 5'-AGAGAGAAAGCAATAAGAAGAAAGCCATCAATGAAAAAGCCGAACAAAACCGGATCCCCGGGTAAATTA-3' and 5'-GTTACAATATAGAAGTTTATACAGTAGAGCTATACAGGATAATGGAAGTGAATTCGAGCTCGTTTAAAC-3'. The PCR product was used to transform the yeast W303-1a (*MATa leu2-3,112 trp1-1 can1-100 ura3-1 ade2-1 his3-11*) by homologous recombination. The recombination was confirmed by PCR and Western blot using anti-HA antibody. The resulting transformant was designated as YH-2 (*MATa leu2-3,112 trp1-1 can1-100 ura3-1 ade2-1 his3-11 Sec62-HA::TRP1*). The YH-2 strain did not show any growth defects at either 30 or 37 °C (data not shown).

To generate the C-terminal MBP-tagged Sec63 construct, PCR was carried out using pFA6a-MBP-HIS3MX6 (14) as a template. The primers were AACTGATATCGATACGGATACAGAAGCTGAAGATGATGAATCACCAGAAATGAAATCGAAGAAGGTAA (forward primer for Sec63) and AATATATACGTCTAAGAGCTAAAATGAAAACTATACTAATCACTTATATGAATTCGAGCTCGTTTAAAC (reverse primer for Sec63). The PCR product was used to transform YH-2 (*MATa leu2-3,112 trp1-1 can1-100 ura3-1 ade2-1 his3-11 Sec62-HA::TRP1*) by homologous recombination. The recombination was confirmed by PCR and Western blot using anti-MBP antibody. The resulting transformant was designated as YH-3 (*MATa leu2-3,112 trp1-1 can1-100 ura3-1 ade2-1 his3-11 Sec62-HA::TRP1 Sec63-MBP::HIS3*). The YH-3 strain did not show any growth defects at 30 or 37 °C (data not shown).

To generate the C-terminal FLAG-tagged Sec63, Sec71, Sec72, Sec61, Sbh1, and Sss1 constructs, PCR was carried out using pFA6a-3xFLAG-HIS3MX6 as a template (13), which was a kind gift from Dr. Rolf Sternglanz (Department of Biochemistry and Cell Biology, Stony Brook University). The primers were AACTGATATCGATACGGATACAGAAGCTGAAGATGATGAATCACCAGAAATGAAATCGAAGAAGGTAA (forward primer for Sec63), AATATATACGTCTAAGAGCTAAAATGAAAACTATACTAATCACTTATATGAATTCGAGCTCGTTTAAAC (reverse primer for Sec63), GTATTAAAGAGTGGGAGCTGAAATAATAATGATGGAAGATTAGTCAATCGGATCCCGGGTTAATTA (forward primer for Sec71), TTTAAATAAAACTGAACGAGCGAATACATATCTTTGCACACAGTAGGCAGAATTCGAGCTCGTTTAAAC (reverse primer for Sec71), GAGCCCTTTTAAATAGAACTGCAAGAAATCTGGCCGAATATAACGGTGAACGGATCCCGGGTTAATTA (forward primer for Sec72), TAGCATAGAGACATATCAAGAAAAGGCTAAAATATCTTCGGTTATGCACCGAATTCGAGCTCGTTTAAAC (reverse

primer for Sec72), AGGAAGGTGGGTTTACTAAGAACTCGTTCCAGGATTTTCTGATTTGATGCGGATCCCGGGTTAATTA (forward primer for Sec61), GTGGCTAAATGCGATTTTTTTTTTCTTTGGATATTATTTCATTTTATATGAATTCGAGCTCGTTTAAAC (reverse primer for Sec61), TTTCTGTTGTTGCATTACATGTTATTCTAAAGTTGCCGGTAAGTTATTTCCGGATCCCCGGTTAATTA (forward primer for Sbh1), GTTTTGTCAAATAGGGTGGATAAAAGCTGAATCATTACTGAAGAAAATTCGAATTCGAGCTCGTTTAAAC (reverse primer for Sbh1), TTGGTTACGCCATCAAGTTGATTCATATCCAATCAGATACGTTATTGTTTCGGATCCCCGGGTAAATTA (forward primer for Sss1), and TTTTTGGTTCTGGTTCGGTTGTTTTATTTTTTCTCGTCTTTTATCTTTGAATTCGAGCTCGTTTAAAC (reverse primer for Sss1). The PCR products were used to transform YH-2 by homologous recombination. The recombination was confirmed by PCR and Western blot using anti-FLAG antibody. The resulting transformants were designated as YH-4 (*MATa leu2-3,112 trp1-1 can1-100 ura3-1 ade2-1 his3-11 Sec62-HA::TRP1 Sec63-FLAG::HIS3*), YH-5 (*MATa leu2-3,112 trp1-1 can1-100 ura3-1 ade2-1 his3-11 Sec62-HA::TRP1 Sec71-FLAG::HIS3*), YH-6 (*MATa leu2-3,112 trp1-1 can1-100 ura3-1 ade2-1 his3-11 Sec62-HA::TRP1 Sec72-FLAG::HIS3*), YH-7 (*MATa leu2-3,112 trp1-1 can1-100 ura3-1 ade2-1 his3-11 Sec62-HA::TRP1 Sec61-FLAG::HIS3*), YH-8 (*MATa leu2-3,112 trp1-1 can1-100 ura3-1 ade2-1 his3-11 Sec62-HA::TRP1 Sbh1-FLAG::HIS3*), and YH-9 (*MATa leu2-3,112 trp1-1 can1-100 ura3-1 ade2-1 his3-11 Sec62-HA::TRP1 Sss1-FLAG::HIS3*). The YH-4, -5, -6, -7, -8, and -9 strains did not show any growth defects at 30 or 37 °C (data not shown).

**Purification of the Yeast Post-translocon**—The yeast strain (YH-2) was grown in 12 liters of YPAD medium at 30 °C for 20 h. The microsomes were prepared as described previously (15). One hundred of A<sub>280</sub> in 1% SDS was defined as 2 eq/ml (15). Ten ml of microsomes (20,000 eq) were incubated with 10 ml of 10 mM Tris-HCl, pH 7.4, 1.0 M NaCl, 20% (v/v) glycerol, 10 mM MgCl<sub>2</sub>, 2 mM EDTA, and 3% (w/v) digitonin for 30 min on ice. After centrifugation at 100,000 × g for 30 min, the supernatant was diluted 3-fold with 10 mM Tris-HCl, pH 7.4, 500 mM NaCl, 10% glycerol, 5 mM MgCl<sub>2</sub>, and 1 mM EDTA and then incubated with 1 ml of anti-HA gel at 4 °C for 2 h. After washing the beads three times with 3 volumes of 10 mM Tris-HCl, pH 7.4, 500 mM NaCl, 10% glycerol, 0.2% digitonin, and 1 mM MgCl<sub>2</sub>, the beads were further washed twice with 10 volumes of Buffer A (10 mM Tris-HCl, pH 7.4, 100 mM NaCl, 10% glycerol, 1 mM MgCl<sub>2</sub>, and 0.2% digitonin). The post-translocon was eluted two or three times with Buffer A containing 0.3 mg/ml HA peptide for 30 min at room temperature. The yield of the post-translocon was ~50 μg/liter of cell culture as judged by SDS-PAGE/silver staining using BSA as a standard.

The eluate was diluted 2-fold with Buffer B (10 mM Tris-HCl, pH 7.4, 10% glycerol, 1 mM MgCl<sub>2</sub>, and 0.2% digitonin) and subjected to Q-Sepharose. After washing the beads three times with Buffer B, the post-translocon was eluted with Buffer B containing 1.0 M NaCl. To exchange the buffer, the fraction was run through a Zeba Spin desalting column (Thermo Scientific)

## Characterizations of the Yeast Post-translocon

equilibrated with 10 mM Tris-HCl, pH 7.4, 100 mM NaCl, 0.5 mM MgCl<sub>2</sub>, and 0.2% digitonin.

**Blue Native-PAGE**—Purified post-translocon was analyzed as described previously (15). In brief, the post-translocon in 10 mM Tris-HCl, pH 7.4, 100 mM NaCl, 0.5 mM MgCl<sub>2</sub>, and 0.2% digitonin was mixed with 0.7% digitonin, 0.01% Ponceau S, and 5% glycerol at the final concentrations. The mixture was subjected to BN-PAGE either in imidazole buffer system (16) or in Bis-Tris buffer system, according to the manufacturer's instructions (Invitrogen).

For BN-PAGE analysis of the digitonin-solubilized microsomes, YH-7 was transformed with pZCSEC61-L6 (K273D/R275D/K284D), pZCSEC61-L8 (R406E), or pZCSEC61-L6L8 (R275E/R406E) (6). The cells were grown in medium lacking leucine to approximately an absorbance at 600 nm, and the microsomes were solubilized in buffer (10 mM Tris-HCl, pH 7.4, 500 mM NaCl, 5 mM MgCl<sub>2</sub>, 1.5% digitonin, and 10% glycerol). After ultracentrifugation at 100,000 × *g* for 20 min, the supernatant was diluted 10-fold with 10 mM Tris-HCl, pH 7.4, 1% digitonin, and 10% glycerol. The sample was mixed with BN-PAGE sample buffer at a ratio of 25:1 (v/v) (16) and immediately subjected to BN-PAGE. After the BN-PAGE, the proteins were transferred to a PVDF membrane. Excess Coomassie Brilliant Blue G-250 was removed from the membrane by incubation for 5 min in 50% methanol, 10% acetic acid. The membrane was then denatured in 62.5 mM Tris-HCl, pH 6.8, 2% SDS, and 0.7% β-mercaptoethanol at 60 °C for 30 min, prior to blocking the membrane with 5% skim milk.

**Detergent Treatment of the Purified Post-translocon**—The purified post-translocon (5–10 nm) was adjusted to 10 mM Tris-HCl, pH 7.4, 100 mM NaCl, 10% glycerol, 0.7% digitonin, and 0.5 mM MgCl<sub>2</sub>. The mixture was incubated with 0–1.0% (w/v) of Triton X-100 for 15 min on ice. After the addition of BN-PAGE sample buffer (0.01% Ponceau S and 5% glycerol), the mixture was immediately subjected to BN-PAGE in the Bis-Tris buffer system as described above. The gel was analyzed either by silver staining or by Western blotting with anti-HA and biotinylated anti-FLAG antibodies.

**Cysteine Labeling**—The purified post-translocon complex (10 pmol of cysteine residues) was incubated in 10% TCA for 30 min on ice. After centrifugation at 18,000 × *g* for 15 min, the pellet was washed once with ice-cold acetone, followed by standing at room temperature until all of the acetone evaporated. The dried pellet was dissolved in 100 mM Tris-HCl, pH 7.4, and 1% SDS at a concentration of 0.5 mM of cysteine. The supernatant was incubated with 5 mM tris (2-carboxyethyl) phosphine for 1 h at room temperature followed by incubation with 10 mM Alexa Fluor 680 C2 maleimide (Invitrogen) for 1 h at room temperature and further incubated for 16 h at 4 °C. The reaction mixture was analyzed by SDS-PAGE and detected by an Odyssey Infrared Imaging System (LI-COR Biosciences).

**STEM Mass Measurement**—STEM was performed in the Brookhaven National Laboratory STEM user facility (Upton, NY). STEM was operated at 40 kV with a magnification of 125,000 and a scanning step of 10 Å. Tobacco mosaic virus was included during specimen preparation as an internal quality control. We subtracted the background of the STEM images in the Windows-based program PCMASS (17), manually selected

1696 particles from 24 cryo-images of 512 × 512 pixels and measured their masses, and then calculated the means and standard deviations of the masses.

**EM Image Acquisition**—The post-translocon particles were visualized by both negative staining and cryo-EM. The negatively stained grids were prepared at a sample concentration of 0.02 mg/ml. Cryo-EM grids of the sample were prepared using the Vitrobot (FEI, Hisbrone, CO) with a specimen chamber humidity of 90% and a temperature of 11 °C. A 4.5-μl sample droplet at 0.05 mg/ml concentration was applied to a quantifoil EM grid and rapidly plunged into liquid ethane after blotting off excess fluid in the Vitrobot. Both the negatively stained grid and the samples embedded in vitreous ice were imaged in the JEOL 2010F electron microscope operating at 200 kV at a magnification of 60,000× and with an underfocus value that varied from 1.0 to 3.5 μm. The images were recorded in low dose conditions (15 e/Å<sup>2</sup>). The cryo-images were recorded on Kodak SO-163 negative film that was developed for 12 min in full-strength Kodak D-19 developer at 20 °C. The micrographs inspected as without drift and astigmatism were digitized with a Nikon Supercool scanner 8000ED at a step size of 7.3 μm and further binned to 12.7 μm for image processing. This corresponds to a pixel size of 2.12 Å at the sample level. All of the images of the negatively stained particles were acquired by a 4K × 4K pixels CCD camera at the magnification of 60,000. After magnification calibration for the CCD camera, the pixel size of the images is 1.76 Å/pixel. Further particle processing and image analysis were based on 2× binned particle images (3.52 Å/pixel).

**Image Processing and Three-dimensional Reconstruction**—The software packages EMAN (18) and SPIDER (19) were used for image processing. We manually selected 5590 and 10610 negatively stained particle images from the post-translocon and the MBP-fused post-translocon samples, respectively. We performed reference-free two-dimensional image classification on these images and calculated averaged images based on classification results. Several three-dimensional models were calculated from selected two-dimensional averages based on the common line technique. These models were refined against the raw particle images, and eventually one model was selected, based on the overall consistence between the reprojections and the reference-free two-dimensional averages. The cryo-EM data set of the post-translocon contained 14920 particles. We collected a second cryo-data set containing 19452 particles for the purpose of structure validation. The three-dimensional model derived from the stained data set was used as starting model to refine the two cryo-data sets. The refined three-dimensional maps from two independent data sets were virtually the same. The resolution of the refined maps was estimated by Fourier shell correlation of the two separately calculated maps. The three-dimensional EM maps were low pass filtered to an estimated resolution of 20 Å. Surface rendering of the EM maps and docking of atomic structures were carried out in the University of California, San Francisco Chimera (20).

## RESULTS

**Purification of the Post-translocon**—Because Sec62 is known to be an essential component for the active post-translocon

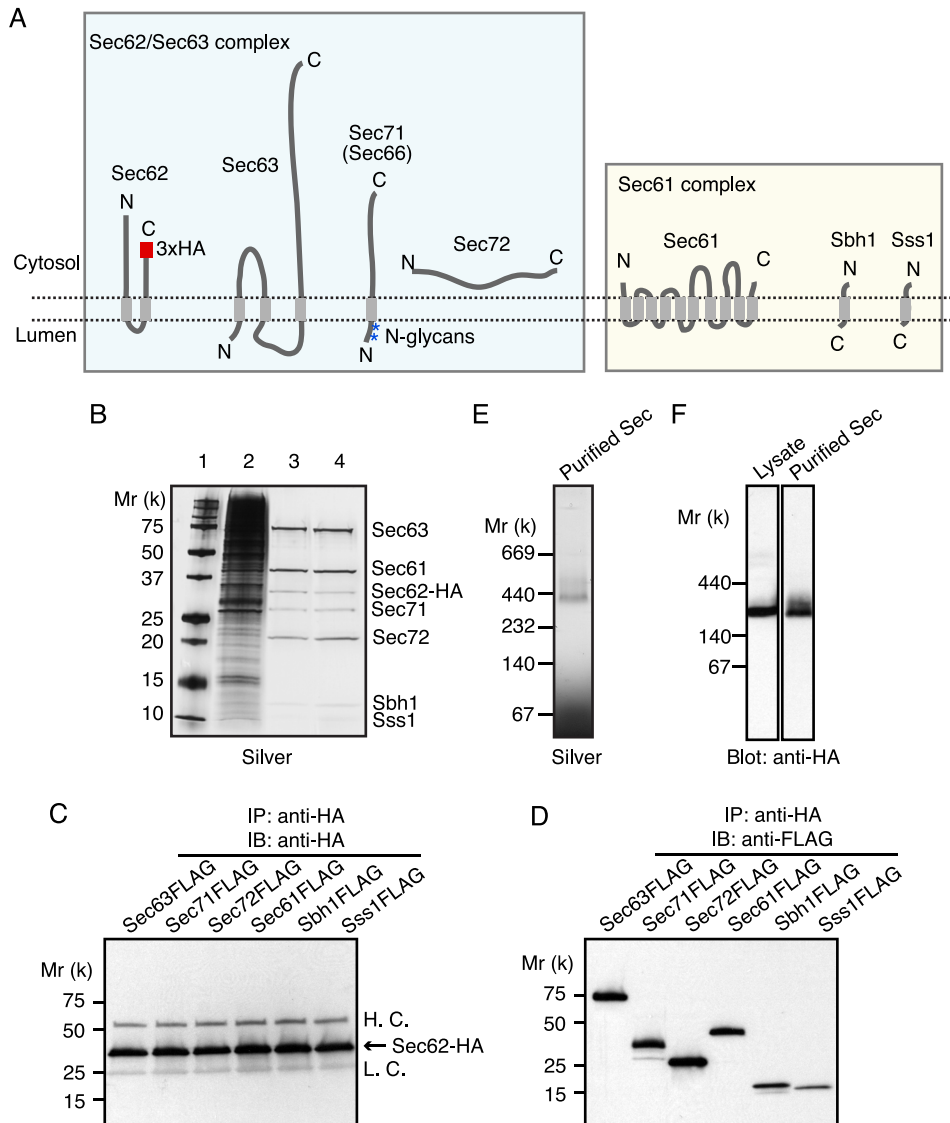


**FIGURE 1. Purification of the post-translocon from yeast.** *A*, subunit composition of the post-translocon. The HA tag, transmembrane regions, and luminal and cytosolic locations of the N and C termini of each subunit and *N*-glycan (shown as asterisks) are diagrammed on the figure. Light green and light yellow boxes represent the Sec2/Sec63 complex and the Sec61 complex, respectively. *B*, SDS-PAGE analysis for purification steps of the post-translocon. The Sec2-HA was immunoprecipitated from the digitonin-soluble fraction of the microsomes using anti-HA beads (1 eq/lane, lane 2). The beads were washed and then eluted with HA peptide (800 eq/lane, lane 3). The eluate was subjected to Q-Sepharose anion exchange chromatography. After washing the beads, the Sec2/63 complex was eluted with 1.0 M NaCl (3,000 eq/lane, lane 4). The molecular weight markers are represented in lane 1. The gel was stained with silver. *C* and *D*, immunoprecipitation of the post-translocon containing Sec2-HA and either the FLAG-tagged Sec63, Sec71, Sec72, Sec61, Sbh1, or Sss1. The Sec2-HA was immunoprecipitated with anti-HA antibody from the digitonin-solubilized microsomes. The immunoprecipitate was analyzed by SDS-PAGE, followed by Western blot with anti-HA (*C*) and anti-FLAG (*D*) antibodies. *H. C.* and *L. C.*, heavy and light chains of IgG, respectively. *E* and *F*, blue native-PAGE analysis for purification steps of the Sec2/63 complex. *E*, the HA peptide-eluate fraction from anti-HA beads was analyzed (300 eq/lane) and stained with silver. *F*, the fractions as shown in *B* (lanes 2 and 3) were subjected to blue native-PAGE and analyzed by Western blot using anti-HA antibody. *IP*, immunoprecipitate; *IB*, immunoblot.

(21), to develop an efficient purification strategy for the heptameric post-translational translocon (post-translocon), we tagged the chromosomal copy of Sec2 with triple HA at its C terminus. The post-translocon was immunoprecipitated from the digitonin-solubilized fraction of the microsomes with anti-HA antibody-conjugated beads and eluted with HA peptide. Remarkably, only the seven expected bands, but not any other contaminating bands, were detected in the eluate as shown by the silver-stained SDS-PAGE (Fig. 1*B*, lane 3). The

Sec2-HA was associated with the FLAG-tagged Sec63, Sec71, Sec72, Sec61, Sbh1, or Sss1 as shown by co-immunoprecipitation (Fig. 1, *C* and *D*), indicating that the purified post-translocon contains all seven known subunits.

We further purified the post-translocon by Q-Sepharose anion exchange chromatography as described previously (12), although improvement in purity was marginal based on SDS-PAGE, possibly because the first immunoprecipitation step had already resulted in a highly pure preparation (Fig. 1*B*, compare lanes 3 and 4). The purified post-translocon migrated to ~350 kDa as single major band in BN-PAGE; the faint and smeared region above the major band might be due to formation of oligomers of the post-translocon (Fig. 1*E*). The Sec2-HA in the digitonin-solubilized microsome co-migrated with that in the purified post-translocon (Fig. 1*F*, compare left and right panels), indicating that the post-translocon was intact after the purification steps.

*The Post-translocon Is Comprised of One Copy of Each of Sec2, Sec3, Sec71, Sec72, Sec61, Sbh1, and Sss1*—Because the subunit stoichiometry of the heptameric post-translocon is not known, we carried out Cys labeling of the purified post-translocon to determine the subunit stoichiometry. Except for Sbh1, the other six subunits all contain Cys residues, ranging in number from 1 to 7. SDS-PAGE of the fluorescently labeled specimen followed by silver staining (Fig. 2, right panel) and fluorescence scanning (Fig. 2, left panel) indicated that all six Cys-containing subunits, *i.e.* Sec63, Sec61, Sec2-HA, Sec71, Sec72, and Sss1, were properly labeled. We quantified the

fluorescence intensity and normalized the intensity by the number of Cys in each subunit. By setting Sec2-HA to 1, the molar ratio for Sec63, Sec61, Sec2-HA, Sec71, Sec72, and Sss1 was ~1:1:1:1:1:1 (Table 1). Although the copy number of Sbh1 was not examined in our experiment, we suggest that the Sec61 complex, the central pore of the post-translocon, also has a unit molar ratio: *i.e.* Sec61:Sbh1:Sss1 is 1:1:1, because its bacterial homolog SecYEG complex is composed of one copy of each of SecY, SecE, and SecG (5).

## Characterizations of the Yeast Post-translocon

Assuming one copy of each of the seven subunits in the post-translocon, the calculated mass is  $\sim 230$  kDa. To provide an independent assessment of the stoichiometry of the complex, we measured the molecular mass of the purified post-translocon by scanning transmission electron microscopy (STEM) (Fig. 3) (17). The mass of the post-translocon, averaged from  $\sim 1700$  individual measurements, was found to be 287 kDa, with a standard deviation of 42 kDa. This result is consistent with the unit stoichiometry of the heptameric complex, as suggested by the Cys labeling experiment. The difference of  $\sim 57$  kDa between the measured and the calculated masses may be attributed to the digitonin and residual lipid molecules surrounding

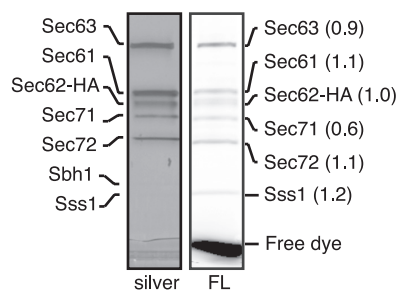


**FIGURE 2. Subunit stoichiometry of the post-translocon.** The purified post-translocon was denatured, reduced, and subsequently labeled with the maleimide containing a fluorescent label. The labeled samples (1 pmol) were analyzed by SDS-PAGE followed either by silver staining (*left panel*) or by direct detection of the fluorescence intensity (*right panel*). The protein amount was estimated by SDS-PAGE/silver staining using BSA as a standard. Individual subunits were identified based on their molecular weight. The molar ratios of Cys, as indicated in *parentheses*, were calculated from fluorescent intensity of each subunit divided by the number of Cys in that subunit. Sec62-HA was set to 1.0.

**TABLE 1**  
Subunit stoichiometry of the post-translocon

Subunit	Relative molar ratio <sup>a</sup>
<b>Sec62/63 complex</b>	
Sec62-HA	1.0 (3)
Sec63	0.9 (7)
Sec71	0.6 (3)
Sec72	1.1 (3)
<b>Sec61 complex</b>	
Sec61	1.1 (3)
Sbh1	-(0)
Sss1	1.2 (1)

<sup>a</sup> Sec62-HA is set to 1.0. The number of Cys residues of each subunit is shown in parentheses.

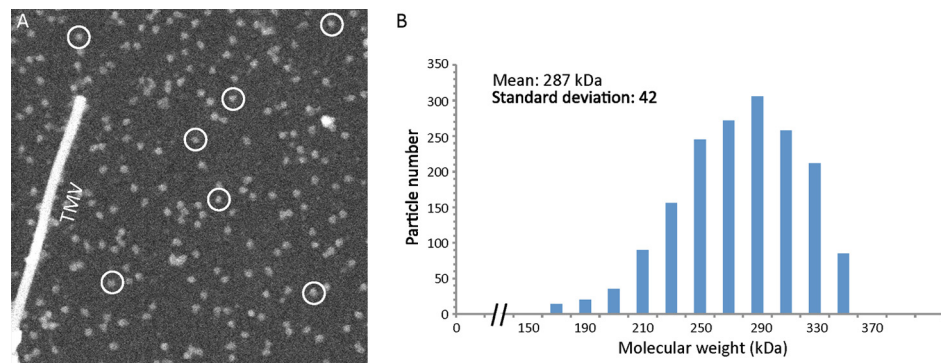


**FIGURE 3. STEM mass measurement of yeast post-translocon supports a unit stoichiometry of the heptameric complex.** *A*, a selected STEM image with seven post-translocon particles encircled randomly as examples. *TMV* indicates the helical rod of the tobacco mosaic virus with a width of 180 Å. *B*, a histogram of the measured particle masses.

the hydrophobic membrane-embedded portion of the post-translocon. Based on the demonstration of seven subunits of the purified complex by the silver-stained SDS-PAGE and mass and stoichiometry analyses, we conclude that the digitonin-solubilized, highly purified yeast post-translocon is comprised of one copy of each of the seven subunits.

**Triton X-100 Treatment Dissociates the Post-translocon into Three Subcomplexes**—The post-translocon was reported to dissociate into two subcomplexes: the Sec61 heterotrimeric complex and the heterotetrameric Sec62/Sec63 complex, by 1.0% of Triton X-100 treatment (12). To gain a more complete pattern of subunit interaction in the post-translocon, we treated the highly purified complex with progressively higher concentrations of Triton X-100, ranging from 0.1% to 1%, and then analyzed by BN-PAGE. We found that the amount of the intact complex gradually decreased with increasing concentrations of the detergent, and at 1.0% Triton X-100, the original complex was virtually absent (Fig. 4*A, O*). Concomitant with the diminution of the original complex, three major bands, corresponding to  $\sim 230$ , 200, and 140 kDa, gradually appeared. These bands are designated as the L (for large), M (medium), and S (small) subcomplexes, respectively.

To investigate the composition of the three subcomplexes, we individually tagged Sec63, Sec71, Sec72, Sec61, Sbh1, and Sss1 with the FLAG epitope and purified each of these FLAG-tagged post-translocons, all containing Sec62-HA as well. The purified and FLAG-tagged complexes were treated with or without 1.0% Triton X-100 and analyzed by BN-PAGE/Western blot with anti-HA and anti-FLAG antibodies, respectively (Fig. 4, *B* and *C*). The Sec62-HA was found in the original and in the L subcomplex (Fig. 4*B* and Table 2). Trace amounts of the Sec62-HA were found at  $\sim 80$  kDa in the presence of Triton X-100. As shown in Fig. 4*C* and Table 2, the FLAG-tagged Sec63, Sec71, and Sec72 subunits were found in the original complex and in the L and M subcomplexes; Sec61, Sbh1, and Sss1 subunits were found in the original complex and in the S subcomplex. These results indicate that the L subcomplex lacks the Sec61 complex. Thus, the L subcomplex is the tetrameric Sec62/Sec63 complex containing Sec62, Sec63, Sec71, and Sec72 subunits. The dissociated Sec61 complex corresponds to the S subcomplex. The M subcomplex is derived from the L subcomplex but lacks Sec62-HA, thus containing the Sec63-Sec71-Sec72 heterotrimer. This trimeric complex has been found in the digitonin-solubilized microsomes (21). Consistent with this assignment, some free Sec62-HA at 80 kDa was observed.

**Production of the MBP-fused Complex for Mapping the Cytosolic Domain of Sec63**—To provide a distinct and sizable feature for orienting the low resolution EM structure of the heptameric complex (see next section), we employed the 38-kDa MBP fusion strategy (14). Among the several constructs attempted, we were able to fuse MBP to the C

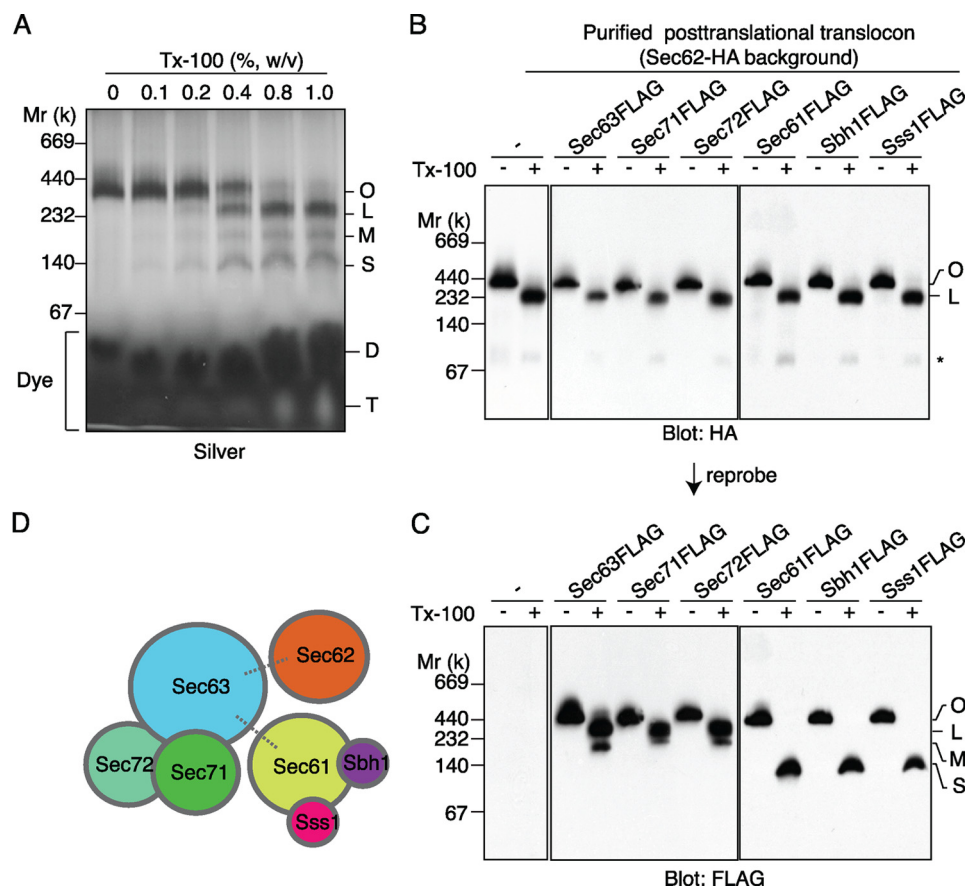


**FIGURE 4. Subcomplex formation of the post-translocon.** *A*, the purified post-translocon (130 eq) was incubated with 0–1.0% (w/v) of Triton X-100 (*Tx-100*) in the presence of 0.7% digitonin and analyzed by BN-PAGE/silver staining. Original (*O*), large (*L*), medium (*M*), and small (*S*) subcomplexes are indicated at the *right* of the panel. Digitonin (*D*) and Triton X-100 (*T*) in the purified post-translocon migrated to the positions indicated at the *right* of the panel. *B* and *C*, treatment of the purified post-translocon containing the FLAG-tagged subunit (30 eq) without (–) or with (+) 1.0% Triton X-100, followed by BN-PAGE/Western blot. The membrane was first probed with anti-HA antibody (*B*) and then reprobbed with anti-FLAG antibody (*C*). An asterisk indicates the free Sec62. *D*, schematic model of subcomplexes of the post-translational translocon. The *dashed lines* represent a Triton X-100-sensitive interaction.

**TABLE 2**  
Subunit compositions of Triton X-100-derived subcomplexes of the post-translocon

Complex <sup>a</sup>	Subunit <sup>b</sup>						
	Sec62	Sec63	Sec71	Sec72	Sec61	Sbh1	Sss1
O	×	×	×	×	×	×	×
L	×	×	×	×			
M		×	×	×			
S					×	×	×

<sup>a</sup> Complexes are designated according to their sizes in BN-PAGE in which the post-translocon was treated with or without Triton X-100.

<sup>b</sup> The subunits in each complex were determined by BN-PAGE/Western blot.

terminus of Sec63 in the yeast cells expressing Sec62-HA. The MBP-fused post-translocon was purified by essentially the same methods used earlier. In the MBP-fused complex, Sec63 was found to up shift up by ~40 kDa in SDS-PAGE (Fig. 5*A*). In the BN-PAGE, the MBP-fused complex was detected as a major band with an approximate increase of 40 kDa over the wild type complex (Fig. 5*B*). These results show that the MBP was successfully fused onto the Sec63, and the fusion protein did not affect the assembly of the heptameric complex.

*Single Particle EM Analysis of the Post-translocon Revealed a Three-lobed Structure*—Because the post-translocon, with total protein mass of only 230 kDa, is relatively small for single particle EM analysis, we first investigated its structure by negative stain EM, which provides higher contrast (Fig. 6). The raw images revealed an asymmetric and open ring-shaped particle that was essentially the same as observed previously by the freeze fracture EM of the native heptameric Sec complex reconstituted in proteoliposomes (22). In the averaged images, however, a consistent three-lobed view was observed, and we labeled the three distinct densities as  $\alpha$ ,  $\beta$ , and  $\gamma$ , respectively (Fig. 6*B*, upper panel). Imaging and computational classification of the MBP-fused heptameric complex derived very similar views with an extra density attached to the  $\beta$  density (Fig. 6*B*, lower panel). Because MBP was fused to the cytosolic C terminus of Sec63, localization of  $\beta$  as the Sec63-containing density suggests that both densities  $\beta$  and  $\gamma$  are in the cytosol and that  $\alpha$  is in the transmembrane region, which is shown by the two parallel *dashed lines* (Fig. 6*B*).

We calculated and refined a low resolution three-dimensional density map from the stained images of the post-translocon complex (Fig. 6*C*). The three-dimensional reconstruction shows a spherical structure of the complex, ~8–10 nm in size and comprised of three large lobes, which are again labeled as  $\alpha$ ,  $\beta$ , and  $\gamma$ , as first identified in the two-dimensional averages. We further attempted cryo-EM on the complex and found that freezing the particles on holey carbon film that was covered with an additional layer of continuous thin carbon film and imaging the cryo-grids at relatively large defocus value (2–4  $\mu\text{m}$  at 200 kV) provided enough contrast for identification of the individual particles in ice (Fig. 7*A*). By iterative refinement of ~15,000 particle images starting with the negative stain three-dimensional model, we obtained a 20-Å resolution cryo-EM three-dimensional map (Fig. 7, *B* and *C*).

The map reveals very similar structural features: a smaller lobe ( $\gamma$ ) attached to two larger lobes of density ( $\alpha$  and  $\beta$ ). The crystal structure of the SecYEG trimer (Protein Data Bank code 1RHZ), a archaeobacterial homolog of the Sec61 complex (5), can be placed into the lower density  $\alpha$ , which has been assigned as the transmembrane region of the complex (Fig. 7*D*). Furthermore, the homolog structure of the Sec63 cytosolic Br1 (Brr2-like) domain (Protein Data Bank code 3HIB) could be placed

## Characterizations of the Yeast Post-translocon

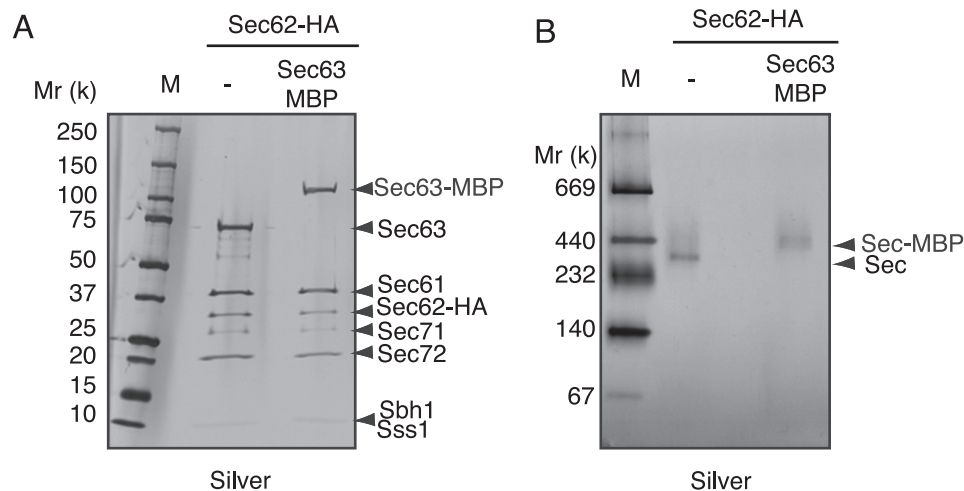


**FIGURE 5. Production of MBP fusion complex for mapping Sec63 by EM.** *A*, SDS-PAGE analysis of the non-MBP-fused and the MBP-fused post-translocon (300 eq/lane). The gel was stained with silver. The Sec subunits were identified based on their molecular weight and indicated at the *right* of the panel. *B*, BN-PAGE/silver stain of the non-MBP-fused and the MBP-fused post-translocon (150 eq/lane). They are indicated as *Sec* and *Sec-MBP*, respectively.

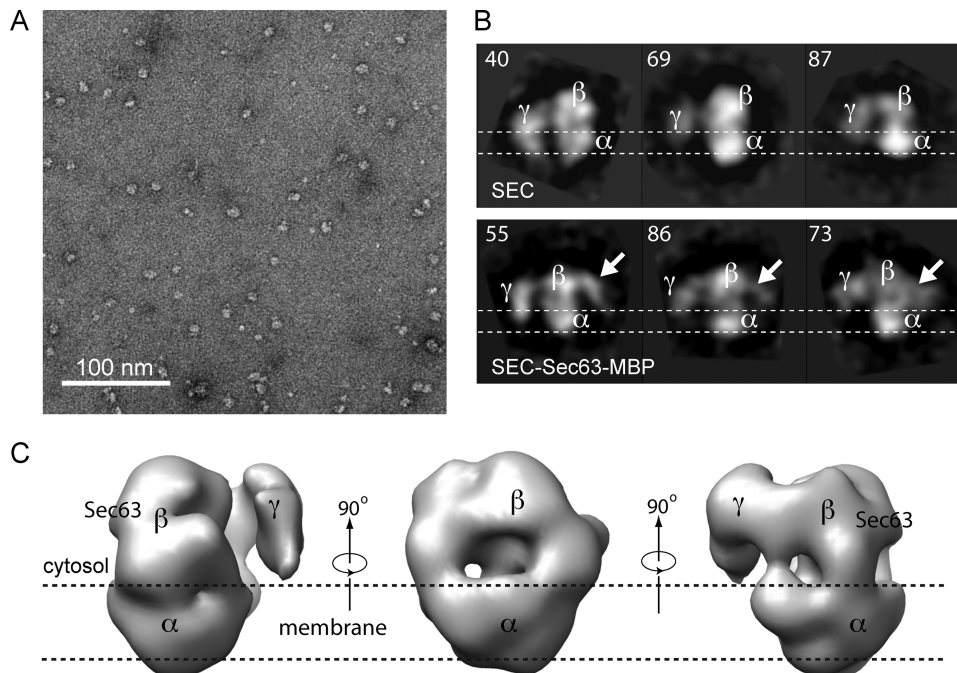


**FIGURE 6. Negative stain EM of the post-translocon and the MBP-fused post-translocon.** *A*, a typical area of the raw micrograph of the post-translocon in negative stain. *B*, two-dimensional class averages of the side views. *Top panel*, the post-translocon; *bottom panel*, the post-translocon with MBP fused to the C terminus of Sec63 subunit. The *white arrows* point to extra clouds of density that are attributed to the fused MBP. Three major density features ( $\alpha$ ,  $\beta$ , and  $\gamma$ ) are labeled. The likely orientation of the particles with respect to the membrane bilayer is indicated. The *numbers* at the *top left corner* of each panel are the numbers of raw particle images used to generate the averages. The density  $\alpha$  is chosen over density  $\gamma$  because transmembrane region because  $\gamma$  is too small to account for the predicted transmembrane mass of the complex. See detail in Fig. 7. *C*, three-dimensional reconstruction of the post-translocon from negatively stained EM images of the purified membrane complex. The three major domains are labeled. The approximate position of Sec63 is also labeled.

into the large Sec63-containing  $\beta$ -lobe of the three-dimensional density (23, 24) (Fig. 7D). The Brl domain is actually a three-domain structure that contains the N-terminal and the middle helical subdomains (63-ND and 63-MD) and the C-terminal immunoglobulin-like subdomain (63-CD) (24). With the placement shown, the C-terminal subdomain of the Sec63 (63-CD) points to the opposite direction of the  $\gamma$ -density, which is

consistent with our finding that the MBP density, fused to the C terminus of Sec63, is at the opposite side of density  $\gamma$  in cytosolic region (Fig. 6B, *lower panel*). The N-terminal helical subdomain of Sec63 (63-ND) is located just above the membrane bilayer, such that the predicted three transmembrane helices at the N terminus of Sec63 would be able to insert into the membrane. We note that the EM map is of low resolution and lacks structural detail. Therefore, the placement of the crystal structures is more qualitative than a quantitative fitting. In such an assignment, the smaller and flexible density  $\gamma$  is likely occupied by Sec71/Sec72, which have most of their densities in the cytosolic side (Fig. 7, C and D). The position of Sec62 is uncertain but likely occupies the region between Sec61 and Sec63, as labeled in the second panel of Fig. 7D. The peripheral location of Sec62 might explain the formation of the stable M subcomplex (Fig. 4) (21).

*The Sixth Cytosolic Loop of Sec61 Is Involved in Assembly of the Post-translocon*—The sixth and eighth cytosolic loops (L6 and L8, respectively) of Sec61 that are highly exposed to the cytosol (25) have been implicated in both co- and post-translational translocation processes (6). Point mutation in the L8 loop inhibits binding of Sec61 to the ribosomes (6, 7). However, the precise mechanism by which these loops are engaged in the post-translational translocation process is unknown. According to our model, we found that the Brl domain of Sec63 that is required for formation of the post-translocon (21) is adjacent to the cytosolic region of Sec61 (Fig. 7). Therefore, we hypothesized that these loops may be important for assembly of the post-translocon. To test this hypothesis, we first developed a novel method. The yeast

cells expressing both Sec62-HA and Sec61-FLAG were transformed with plasmid encoding the nontagged Sec61. We found that an antibody that had been raised against C-terminal peptide of the Sec61 (12) recognizes only nontagged Sec61 but not the Sec61-FLAG (Fig. 8A, compare *middle* and *right panels*). Therefore, we could distinguish the FLAG-tagged Sec61 from the nontagged version by Western blot analysis.

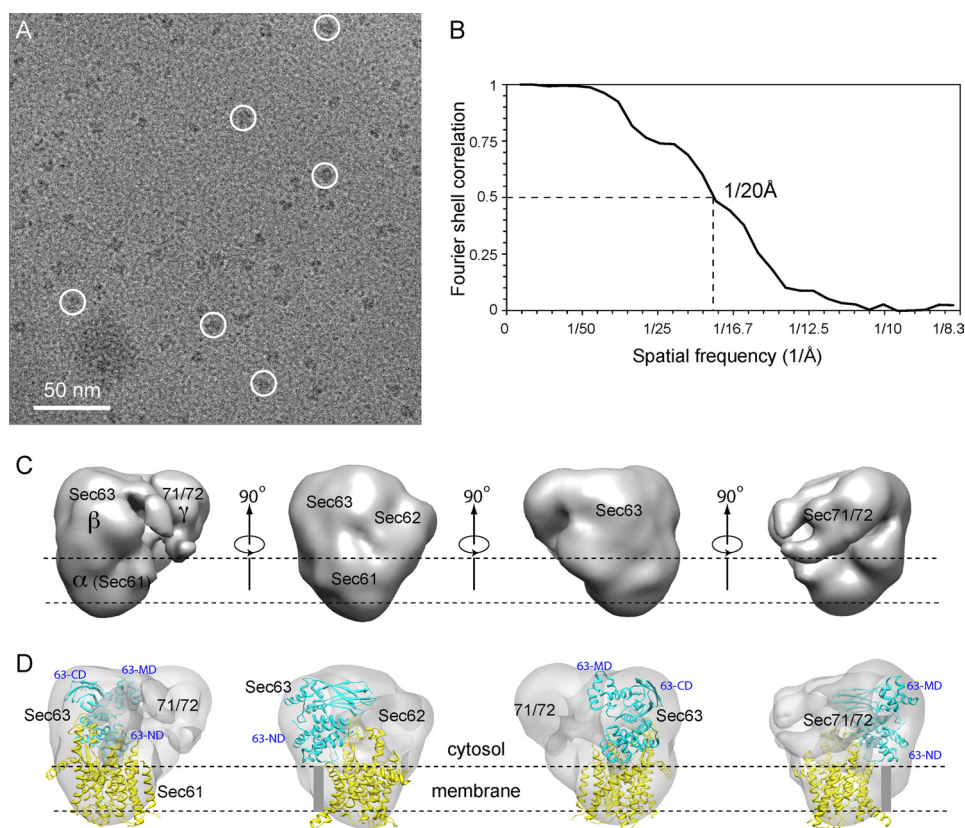


FIGURE 7. **Cryo-EM of the post-translocon at ~20-Å resolution.** *A*, Raw image with six individual particles highlighted in white circles. *B*, Fourier shell correlation. *C*, surface rendered side views of the three-dimensional cryo-EM map. *D*, tentative docking of Sec61 heterotrimer in yellow and Sec63 cytosolic domain homolog structure in cyan. A gray bar represents a hypothetical transmembrane helices of Sec63 that precede the N-terminal subdomain (63-ND) of the cytosolic Brl domain of Sec63. The middle helical (63-MD) and the C-terminal immunoglobulin-like subdomains (63-CD) are labeled.

The digitonin-solubilized microsomes were prepared from the cells containing empty vector and analyzed by BN-PAGE, followed by Western blot. As shown in Fig. 8*B* (lane 5), the Sec61-FLAG migrated at 140 kDa as the Sec61 complex (Sec61) (21), and it also co-migrated with Sec62-HA, forming the post-translocon (Fig. 8*B*, compare lanes 1 and 5, SEC) (21). Another Sec61-containing complex, previously defined as SEC' (21), was also observed (Fig. 8*B*, lane 5): the SEC' complex is composed of Sec63, Sec71, Sec72, Sec61, Sbh1, and Sss1 (21). When the nontagged Sec61 was expressed, it was found in the SEC and SEC' complexes (Fig. 8*B*, lane 4). However, the FLAG-tagged Sec61 was no longer associated with the SEC and SEC' complexes, and it existed as the Sec61 complex (Fig. 8*B*, lane 6). These results indicate that although Sec61-FLAG is capable of formation of the post-translocon (see also Fig. 4), it has a lower affinity for the complex than the nontagged Sec61.

Using this method, we examined the ability of the plasmid-encoded loop mutant Sec61 to form the post-translocon in cells expressing endogenous Sec61-FLAG (Fig. 8*C*). The R406E mutant Sec61, impaired in ribosome binding (6, 7), was found to be associated with the SEC and SEC' complexes, to the same extent as the wild type Sec61 (Fig. 8*C*, compare lanes 5 and 6). As expected, the Sec61-FLAG did not form these complexes (Fig. 8*C*, lanes 9 and 10). The L6 loop triple mutant (L6DDD, K273D/R275D/K284D) showed decreased formation of the SEC and SEC' complexes (Fig. 8*C*, compare lanes 5 and 7).

Interestingly, the Sec61-FLAG could be incorporated into the SEC and SEC' complexes in the presence of the L6 loop triple mutant (Fig. 8*C*, lane 11). Similar results were observed in the L6 and L8 double-loop mutant (L6L8EE, R275E/R406E) (Fig. 8*C*, lanes 8 and 12). As expected, the Sec62 remained associated with the SEC complex (Fig. 8*C*, lanes 1–4), because the Sec61-FLAG is still able to form the SEC complex, instead of the L6 triple and L6L8EE mutants. Densitometry of the Sec61 trimer showed that 3% of the wild type Sec61 formed the trimer (Fig. 8*C*, lane 5). We found that 4% of L8 single mutant (R406E) formed the trimer (Fig. 8*C*, lanes 6 and 7). The effect of L6L8DD mutant on formation of the Sec61 trimer was more significant (49%) than L6DDD mutant (13%) (Fig. 8*C*, lanes 7 and 8). These results suggest that both L6 and L8 loops are involved in the assembly of the protein-conducting channel Sec61 complex and the Sec62/63 complex. However, the L6 loop is probably the primary site for the assembly,

because the L8 mutant did not show increased formation of the Sec61 trimer.

## DISCUSSION

We have found that the purified yeast post-translocon contains a single Sec61 translocation channel. This is consistent with the *in vivo* study in which only one Sec61 molecule was photocross-linked to the signal sequence of prepro- $\alpha$ -factor during the post-translational translocation in yeast membrane (26). In the crystal structure of the prokaryotic post-translational translocon, the SecYEG-SecE complex, only a single SecYEG is present (27). Although binding partners of the yeast and prokaryotic systems are different, it is interesting that both post-translational translocation systems contain a single channel. In the co-translational translocation system, the translating ribosome is bound to a single copy of the Sec61/Ssh1 complex (7). Therefore, the single channel might be a universal mechanism for protein translocation. However, in the bacterial plasma membrane, although a single copy of the SecYEG complex is active in post-translational translocation, there is ample evidence that translocation might be mediated by two or more copies of the SecYEG complex (28–32). Therefore, the issue of oligomeric state of the translocating channel in the membrane may not yet have been settled.

Cryo-EM analysis revealed two large lobes of the yeast post-translocon that could be located in the cytosol. The cytosolic

## Characterizations of the Yeast Post-translocon

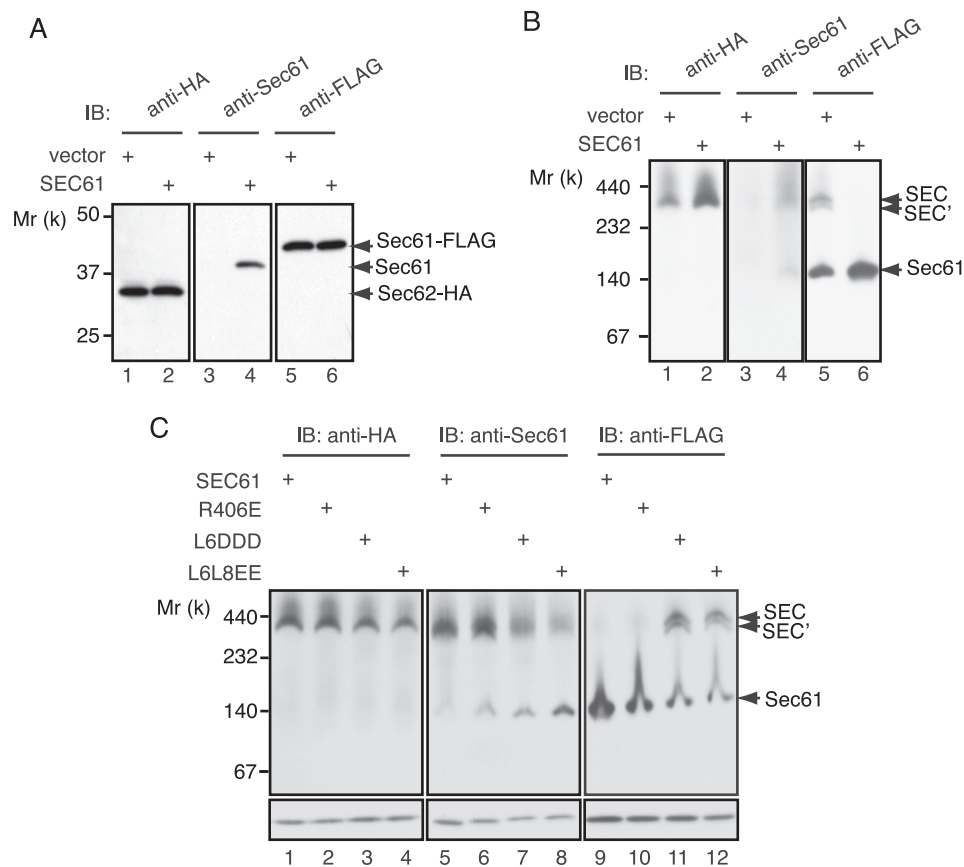


**FIGURE 8. Effects of the cytosolic loops of Sec61 on formation of the post-translocon.** *A*, SDS-PAGE/Western blot analyses of the digitonin-solubilized microsomes. The microsomes were prepared from cells expressing Sec62-HA and Sec61-FLAG that were transformed with either empty vector (vector; lanes 1, 3, and 5) or plasmid encoding wild type Sec61 (SEC61; lanes 2, 4, and 6). The PVDF membranes were blotted with anti-HA antibody for the Sec62-HA marker (left panel), anti-Sec61 antibody for the nontagged Sec61 marker (middle panel), and anti-FLAG antibody for the Sec61-FLAG marker (right panel). *B*, the same sample as in *A* was analyzed by BN-PAGE, followed by Western blot with anti-HA (left panel), anti-Sec61 (middle panel), and anti-FLAG (right panel) antibodies. The post-translocon, the Sec62-dissociated complex, and the Sec61 complex are indicated as SEC, SEC', and Sec61, respectively. *C*, BN- and SDS-PAGE/Western blot analyses of the digitonin-solubilized microsomes from cells containing the wild type (SEC61; lanes 1, 5, and 9), R406E (lanes 2, 6, and 10), L6DDD (lanes 3, 7, and 11), and L6L8EE (lane 4, 8, and 12) mutants Sec61. Upper panels, BN-PAGE; lower panels, SDS-PAGE. IB, immunoblot.

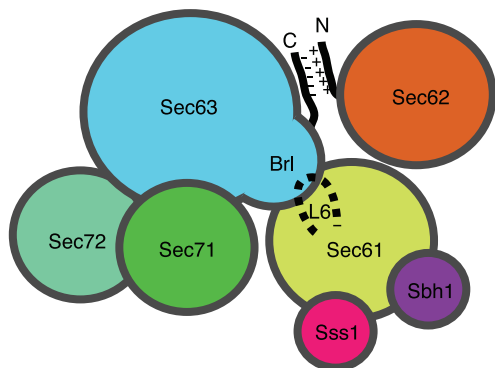


**FIGURE 9. Hypothetical model for formation of the post-translocon.** *A* cytosolic view of the post-translocon is depicted. See details in main text.

domain of the post-translocon is mainly composed of the tetrameric Sec62/Sec63 complex and has two functions: assembly of the functional co- and post-translocons (21) and recruitment of nascent chain to the Sec61 channel (10, 33, 34). Interestingly, we found the cytosolic Brl domain of Sec63 subunit juxtaposed

to the Sec61 complex. This domain is required for tethering the Sec61 complex within the post-translocon (SEC) and SEC' complexes (21) and has been implicated in protein-protein interaction (21, 24). Therefore, we suggest that the Brl domain may directly interact with the Sec61 complex. Mutagenesis of Sec61 identified that the cytosolic L6 loop is involved in assembly of the post-translocon (SEC) and SEC' complexes. Although tagging of the C terminus of Sec61 diminished its binding activity to the SEC and SEC' complexes, the L6 loop is probably the primary binding site for the SEC and SEC' complexes because the L6DDD mutant (K273D/R275D/K284D) failed to associate with the SEC and SEC' complexes. Based on these findings, we propose that the L6 loop can be an excellent candidate as a binding site for the Brl domain of Sec63.

The L6 loop did not significantly affect the ribosome-binding activity of Sec61 (6, 7). However, point mutations in this loop including the L6DDD mutant inhibited translocation of both a SRP-dependent substrate (dipeptidyl aminopeptidase B) and the SRP-independent substrates (carboxypeptidase Y and Gas1) (6). Because the SEC' complex is required for the co-translational translocation process (21), our observation that the L6 loop mutant showed decreased formation of the SEC and SEC' complexes supports the translocation defects of this mutant in both co- and post-translational translocation processes.

In the co-translational translocation pathway involving in the ribosomes and Sec61 complex, the Sec61 subunit uses the highly conserved L8 loop to bind to the exit tunnel of the ribosomes (6, 7). Although the post-translocon contains the Sec61 complex, it does not bind to the ribosome (35). Therefore, we propose that the L8 loop is shielded by cytosolic domains of the Sec62/Sec63 complex. This proposal is supported by the fact that the L6 loop, only ~15 Å away from the L8 loop (6), is engaged in assembly of the post-translocon. Our proposal potentially explains why only fully synthesized nascent chains are targeted to the post-translocon, because the post-translocon has lost its ribosome binding capability.

Based on our EM map and the subunit dissociation pattern of the post-translocon, together with the previous studies on interaction between Sec subunits (36) and signal sequence of prepro- $\alpha$ -factor (33), we propose a model for the architecture of the post-translocon in Fig. 9. The post-translocon is com-

posed of two major structural units: the trimeric Sec61 complex and the tetrameric Sec62/Sec63 complex, as reported previously (12). Interaction between the positively charged N terminus of Sec62 with the negatively charged C terminus of Sec63 contributes to formation of the post-translocon (36). The peripheral location of Sec62 is suggested based on the dissociation pattern of the post-translocon. The Sec63 could be the major interaction partner for the Sec61 complex via the cytosolic Brl domain of the Sec63 subunit. The Sec61 subunit may utilize the sixth cytosolic loop to bind to the Brl domain. During post-translational translocation of prepro  $\alpha$ -factor, Sec61, Sec62, and Sec71 are in contact with the signal sequence of prepro  $\alpha$ -factor (33). As such, Sec62 and Sec71 are located adjacent to the Sec61 complex. Because deletion of Sec71 causes rapid degradation of Sec72 in cells (37), it is likely that this protein binds to Sec72 to protect it from degradation. The Sec71 and Sec72 subunits form a stable complex with Sec63 by an unknown mechanism.

*Acknowledgments*—We thank Dr. Tom A. Rapoport (Harvard Medical School) for anti-Sec61 antibody; Dr. Reid Gilmore (University of Massachusetts Medical School) for plasmids encoding the wild type and the L6 and L8 mutants Sec61; Drs. Guangtao Li and Gang Zhao (Stony Brook University) for discussion; and Aya Harada (Stony Brook University) for technical assistance. We also thank Beth Lin for help with STEM mass analysis.

## REFERENCES

- Rapoport, T. A. (2007) *Nature* **450**, 663–669
- Stroud, R. M., and Walter, P. (1999) *Curr. Opin. Struct. Biol.* **9**, 754–759
- McClellan, A. J., and Brodsky, J. L. (2000) *Genetics* **156**, 501–512
- Wilkinson, B. M., Critchley, A. J., and Stirling, C. J. (1996) *J. Biol. Chem.* **271**, 25590–25597
- Van den Berg, B., Clemons, W. M., Jr., Collinson, I., Modis, Y., Hartmann, E., Harrison, S. C., and Rapoport, T. A. (2004) *Nature* **427**, 36–44
- Cheng, Z., Jiang, Y., Mandon, E. C., and Gilmore, R. (2005) *J. Cell. Biol.* **168**, 67–77
- Becker, T., Bhushan, S., Jarasch, A., Armache, J. P., Funes, S., Jossinet, F., Gumbart, J., Mielke, T., Berninghausen, O., Schulten, K., Westhof, E., Gilmore, R., Mandon, E. C., and Beckmann, R. (2009) *Science* **326**, 1369–1373
- Beckmann, R., Bubeck, D., Grassucci, R., Penczek, P., Verschoor, A., Blobel, G., and Frank, J. (1997) *Science* **278**, 2123–2126
- Deshaies, R. J., Sanders, S. L., Feldheim, D. A., and Schekman, R. (1991) *Nature* **349**, 806–808
- Lyman, S. K., and Schekman, R. (1997) *Cell* **88**, 85–96
- Stirling, C. J., Rothblatt, J., Hosobuchi, M., Deshaies, R., and Schekman, R. (1992) *Mol. Biol. Cell* **3**, 129–142
- Panzner, S., Dreier, L., Hartmann, E., Kostka, S., and Rapoport, T. A. (1995) *Cell* **81**, 561–570
- Longtine, M. S., McKenzie, A., 3rd, Demarini, D. J., Shah, N. G., Wach, A., Brachat, A., Philippsen, P., and Pringle, J. R. (1998) *Yeast* **14**, 953–961
- Li, H., Chavan, M., Schindelin, H., and Lennarz, W. J. (2008) *Structure* **16**, 432–440
- Harada, Y., Li, H., and Lennarz, W. J. (2009) *Proc. Natl. Acad. Sci. U.S.A.* **106**, 6945–6949
- Wittig, I., Braun, H. P., and Schagger, H. (2006) *Nat. Protoc.* **1**, 418–428
- Wall, J. S., and Simon, M. N. (2001) *Methods Mol. Biol.* **148**, 589–601
- Tang, G., Peng, L., Baldwin, P. R., Mann, D. S., Jiang, W., Rees, L., and Ludtke, S. J. (2007) *J. Struct. Biol.* **157**, 38–46
- Shaikh, T. R., Gao, H., Baxter, W. T., Asturias, F. J., Boisset, N., Leith, A., and Frank, J. (2008) *Nat. Protoc.* **3**, 1941–1974
- Petterson, E. F., Goddard, T. D., Huang, C. C., Couch, G. S., Greenblatt, D. M., Meng, E. C., and Ferrin, T. E. (2004) *J. Comput. Chem.* **25**, 1605–1612
- Jermy, A. J., Willer, M., Davis, E., Wilkinson, B. M., and Stirling, C. J. (2006) *J. Biol. Chem.* **281**, 7899–7906
- Hanein, D., Matlack, K. E., Jungnickel, B., Plath, K., Kalies, K. U., Miller, K. R., Rapoport, T. A., and Akey, C. W. (1996) *Cell* **87**, 721–732
- Ponting, C. P. (2000) *Biochem. J.* **351**, 527–535
- Zhang, L., Xu, T., Maeder, C., Bud, L. O., Shanks, J., Nix, J., Guthrie, C., Pleiss, J. A., and Zhao, R. (2009) *Nat. Struct. Mol. Biol.* **16**, 731–739
- Song, W., Raden, D., Mandon, E. C., and Gilmore, R. (2000) *Cell* **100**, 333–343
- Plath, K., Wilkinson, B. M., Stirling, C. J., and Rapoport, T. A. (2004) *Mol. Biol. Cell* **15**, 1–10
- Zimmer, J., Nam, Y., and Rapoport, T. A. (2008) *Nature* **455**, 936–943
- Osborne, A. R., and Rapoport, T. A. (2007) *Cell* **129**, 97–110
- Tam, P. C., Maillard, A. P., Chan, K. K., and Duong, F. (2005) *EMBO J.* **24**, 3380–3388
- Breyton, C., Haase, W., Rapoport, T. A., Kühlbrandt, W., and Collinson, I. (2002) *Nature* **418**, 662–665
- Duong, F. (2003) *EMBO J.* **22**, 4375–4384
- Tziatzios, C., Schubert, D., Lotz, M., Gundogan, D., Betz, H., Schagger, H., Haase, W., Duong, F., and Collinson, I. (2004) *J. Mol. Biol.* **340**, 513–524
- Plath, K., Mothes, W., Wilkinson, B. M., Stirling, C. J., and Rapoport, T. A. (1998) *Cell* **94**, 795–807
- Blatch, G. L., and Lässle, M. (1999) *Bioessays* **21**, 932–939
- Prinz, A., Behrens, C., Rapoport, T. A., Hartmann, E., and Kalies, K. U. (2000) *EMBO J.* **19**, 1900–1906
- Wittke, S., Dünwald, M., and Johnsson, N. (2000) *Mol. Biol. Cell* **11**, 3859–3871
- Feldheim, D., and Schekman, R. (1994) *J. Cell. Biol.* **126**, 935–943